J. Fluid Mech. (2006), *vol.* 557, *pp.* 411–422.
doi:10.1017/S0022112006009669 Printed in the United Kingdom

Turbulent convection at high Rayleigh numbers and aspect ratio 4

By J. J. NIEMELA AND K. R. SREENIVASAN

The Abdus Salam International Center for Theoretical Physics, Strada Costiera 11, 34014 Trieste, Italy

(Received 15 October 2005 and in revised form 9 December 2005)

We report measurements of the Nusselt number, Nu, in turbulent thermal convection in a cylindrical container of aspect ratio 4. The highest Rayleigh number achieved was $Ra = 2 \times 10^{13}$. Except for the last half a decade or so of Ra, experimental conditions obey the Boussinesq approximation accurately. For these conditions, the data show that the $\log Nu$–$\log Ra$ slope saturates at a value close to $1/3$, as observed previously by us in experiments with smaller aspect ratios. The increasing slope over the last half a decade of Ra is inconclusive because the corresponding conditions are non-Boussinesq. Finally, we report a modified scaling relation between the plume advection frequency and Ra that collapses data for different aspect ratios.

1. Introduction

Considerable attention has been given to turbulent Rayleigh–Bénard convection, in part because it is the paradigm for diverse natural phenomena and industrial applications. Rayleigh–Bénard convection occurs when a layer of fluid is sufficiently heated from below and cooled from above that a macroscopic flow is generated, augmenting the molecular transport of heat. Natural phenomena usually occur at very high Rayleigh numbers (Sreenivasan & Donnelly 2000). The Rayleigh number is the characteristic non-dimensional measure of the temperature difference prescribed across the fluid layer, and is defined by $Ra \equiv \alpha \Delta T g H^3/\nu\kappa$, where α is the isobaric thermal expansion coefficient of the fluid in the container, ΔT the temperature difference between the bottom and top walls, g the acceleration due to gravity and H the vertical dimension of the convection cell; ν and κ are, respectively, the kinematic viscosity and the thermal diffusivity of the fluid. The use of low-temperature helium gas as the test fluid has allowed Rayleigh numbers up to 10^{17} to be reached in the laboratory (Niemela *et al.* 2000), much higher than had been previously achieved (Wu 1991; Wu & Libchaber 1992).

However, the experiment of Niemela *et al.*, and others like it (Chavanne *et al.* 2001; Roche *et al.* 2001), had a rather small value of $1/2$ for the diameter-to-height ratio, or the aspect ratio Γ. While it is advantageous to keep the height H large to attain large Ra, it is technically difficult in terms of construction and expensive in terms of helium consumption to increase lateral dimensions correspondingly. Thus, in the experiments just cited, one of the principal features of large-scale flows in nature has been approached, namely high Ra, but the other important feature, namely the large lateral extent, has been abandoned. To remedy this situation somewhat, Niemela & Sreenivasan (2003*a*) increased the aspect ratio to unity while still achieving an Ra of 2×10^{15}, which was more than four orders of magnitude higher than that reported earlier for the same Γ in the pioneering experiments of Wu & Libchaber (1992). There

is no doubt that an even higher aspect ratio would be desirable if the measurements are to be of interest to geophysicists. The present work, combining aspect ratio 4 with a high Ra of up to 2×10^{13}, fills this requirement quite well, although it is not reasonable to claim that it fully approximates a laterally unbounded layer. The combination of moderately large aspect ratio and very high Ra is indeed rare. The closest attempt is that of Wu & Libchaber (1992), who achieved an Ra of almost 10^{10} with $\Gamma = 6.7$.

Mention should be made of measurements covering a large range of Ra from several apparatus of varying aspect ratio (e.g. Goldstein & Tokuda 1979), and those covering lower ranges of Ra but with higher aspect ratio (e.g. Nikolaenko *et al.* 2005), and those others with low Ra and low Γ with considerable flow details mapped out (e.g. Qiu & Tong 2001; Zhou & Xia 2002). Also to be mentioned are numerical simulations of Amati *et al.* (2005) which have pushed the Ra range to increasingly higher values, and the important attempt of Grossmann & Lohse (2002) to understand the flow theoretically. Many other relevant references are cited in Niemela & Sreenivasan (2003*a*).

2. The apparatus

The apparatus is essentially the same as that described earlier in Niemela *et al.* (2000). It was a cylinder of 50 cm diameter, with the height reduced to 12.5 cm, giving the aspect ratio $\Gamma = 4$. The stainless steel sidewall had a thickness of 0.267 cm. The top and bottom plates were made of copper annealed under oxygen-free conditions and 3.8 cm in thickness, with thermal conductivity of the order of $1\,\mathrm{kW\,m^{-1}\,K^{-1}}$ at the measurement temperature. Special efforts were made to heat the plates uniformly, using distributed thin film heater elements. At the bottom plate a constant heat flux was applied, but measurements were initiated only after the resulting plate temperatures reached steady values. Waiting times varied from several hundred to 10^5 cycles of the large-scale circulation, or the mean wind. We have not observed any of the long-term transients reported recently by Chilla *et al.* (2004). The convection cell was insulated by three outer thermal shields at various graded temperatures, residing in a common vacuum space.

The working fluid was helium gas held at a temperature near 5 K. The top plate was linked to a helium bath serving as the cold reservoir, through an adjustable gaseous helium thermal link. Its temperature was maintained constant by means of a resistance bridge and servo.

3. Experimental results

3.1. *Measured heat transport for aspect ratio* 4

We measured the Nusselt number, Nu, where Nu is the ratio of the measured total heat flux to that due to molecular conduction for the same ΔT and H. As in all previous measurements, corrections were made for the small adiabatic temperature gradient across the fluid depth (see Tritton 1988, appendix to chapter 14) and averaging occurred over about 100 cycles of the mean wind. The experimental conditions and the measured Nu are listed in table 1. Two additional corrections seemed necessary to account for the unavoidable finite conductivity of the horizontal plates and the heat leak up the sidewall. We have applied both corrections, as described in the next section. We should point out that the corrections for finite conductivity of the horizontal plates are smaller for cryogenic helium than for conventional fluids.

Q (mW)	ΔT (mK)	T_M (K)	ρ (kg m^{-3})	Ra	Nu	Nu_{corr}	Pr	$\alpha\Delta T$
81.3	151.9	5.026	0.6536	1.10×10^{8}	34.94	32.78	0.69	0.031
126.2	212.2	5.056	0.6584	1.53×10^{8}	38.65	36.37	0.69	0.043
181.2	282	5.091	0.647	1.92×10^{8}	41.53	39.17	0.69	0.057
81.4	115.5	5.008	1.186	2.84×10^{8}	46.24	43.72	0.7	0.024
126.3	163	5.031	1.168	3.83×10^{8}	50.65	48	0.7	0.034
181.2	213.1	5.057	1.191	5.14×10^{8}	55.36	52.59	0.7	0.044
246.4	271.8	5.086	1.175	6.28×10^{8}	58.75	55.89	0.7	0.056
81.2	80.9	4.99	2.485	9.35×10^{8}	66	62.94	0.72	0.018
181.4	167.2	5.034	1.977	1.17×10^{9}	70.88	67.7	0.71	0.036
126.3	114.4	5.007	2.441	1.26×10^{9}	72.37	69.15	0.72	0.025
181.3	150.8	5.024	2.455	1.67×10^{9}	78.56	75.2	0.72	0.033
246.4	191.1	5.046	2.448	2.07×10^{9}	83.91	80.44	0.72	0.042
81.4	56.8	4.978	4.892	2.86×10^{9}	93.57	89.89	0.77	0.014
126.3	79	4.99	5.001	4.16×10^{9}	104.1	100.2	0.77	0.019
181.6	105.7	5.003	4.886	5.24×10^{9}	111.6	107.5	0.77	0.026
181.1	101	5.001	5.387	6.24×10^{9}	116.2	112.1	0.78	0.025
246.6	128	5.014	5.387	7.85×10^{9}	124.5	120.3	0.78	0.032
321.4	164	5.032	4.878	7.95×10^{9}	126.6	122.3	0.77	0.04
321.4	156.7	5.028	5.385	9.51×10^{9}	132.2	127.8	0.78	0.039
406.6	188	5.044	5.387	1.13×10^{10}	139.0	134.5	0.78	0.046
81.4	35.2	4.968	11.16	1.28×10^{10}	146.3	141.7	0.9	0.011
126.2	49	4.975	11.16	1.77×10^{10}	162.5	157.7	0.9	0.016
181.3	65.2	4.983	11.17	2.35×10^{10}	175.0	169.9	0.9	0.021
246.5	81.9	4.991	11.16	2.93×10^{10}	189.0	183.8	0.9	0.026
321.3	100.3	5.000	11.16	3.57×10^{10}	200.7	195.3	0.9	0.032
321.1	92.2	4.996	12.38	4.34×10^{10}	216.6	211.0	0.93	0.031
406.4	110.3	5.005	12.38	5.15×10^{10}	228.6	222.8	0.93	0.037
406.2	104.6	5.002	13.26	5.92×10^{10}	239.6	233.7	0.95	0.037
406.5	94.2	4.997	15.13	7.80×10^{10}	262.8	256.7	1.01	0.036
501.4	99.3	5.299	17.54	9.89×10^{10}	286.5	280.4	1.04	0.038
605.7	116.2	5.458	17.54	1.02×10^{11}	288.5	282.4	1.02	0.042
639.4	111.2	5.456	19.43	1.33×10^{11}	313.4	307.1	1.07	0.043
501.5	82.2	5.291	21.14	1.50×10^{11}	336.5	329.9	1.16	0.037
406.3	70	4.985	20.82	1.67×10^{11}	338.2	331.4	1.22	0.037
500.8	74.7	5.187	23.07	2.08×10^{11}	369.4	362.5	1.27	0.04
605.9	86.8	5.193	23.07	2.40×10^{11}	384.0	377.0	1.26	0.046
501.1	61.8	5.281	27.47	3.10×10^{11}	422.0	415.0	1.46	0.04
501.6	60.3	5.18	27.45	3.47×10^{11}	439.4	432.2	1.51	0.042
691.6	79.8	5.29	27.46	3.96×10^{11}	449.7	442.5	1.45	0.051
690.8	61.6	5.281	32.65	7.06×10^{11}	551.8	544.4	1.84	0.055
501.1	39.9	5.295	36.66	8.61×10^{11}	590.9	583.8	2.25	0.046
691.6	51.5	5.301	36.32	1.04×10^{12}	632.2	625.1	2.19	0.057
846.9	59.7	5.605	39.92	1.06×10^{12}	625.7	619.0	2.08	0.058
691.7	50.4	5.275	36.64	1.14×10^{12}	645.8	638.7	2.28	0.059
981.3	67.5	5.609	39.89	1.18×10^{12}	640.7	634.1	2.07	0.065
721.2	44.7	5.372	40.94	1.58×10^{12}	716.2	709.8	2.64	0.062
721.2	42.7	5.281	40.88	1.20×10^{12}	754.4	748.1	2.94	0.069
845.9	39.7	5.42	46.73	2.90×10^{12}	883.9	879.7	3.4	0.074
912.2	42.2	5.421	46.73	3.07×10^{12}	896.1	892.1	3.39	0.079
846.3	30.5	5.415	51.74	4.61×10^{12}	1091	1091	4.46	0.078
846.3	28.1	5.414	53.31	5.25×10^{12}	1165	1168	4.84	0.079
781.9	25.3	5.388	53.39	5.74×10^{12}	1191	1195	5.25	0.079
721.0	18.4	5.269	53.53	1.15×10^{13}	1467	1482	8.15	0.099
721.0	17.9	5.259	53.55	1.26×10^{13}	1500	1517	8.59	0.103
721.2	12.3	5.256	57.87	2.48×10^{13}	2021	2077	13.44	0.119
721.2	11.6	5.246	57.93	2.87×10^{13}	2119	2184	14.72	0.125

TABLE 1. Experimental parameters from measurements with $\Gamma = 4$. T_M is the mean temperature of the cell. See text for definitions of the other parameters.

3.2. *Corrections*

3.2.1. *Finite conductivity of horizontal plates*

As discussed by Verzicco (2004), the thermal conductivity of the horizontal plates should be very large compared to that of the fluid in order for the plates to maintain constant temperature even in the presence of large turbulent fluctuations. This condition holds quite comfortably for the combination of cryogenic helium and plates made of special copper. However, the *effective* conductivity of helium grows with Ra because of turbulence and can become comparable to that of the plates at very high Ra. The effect is that the plates cannot quickly recover their constant-temperature condition as they would if the conductivity were infinitely large. The problem was also briefly considered by Chaumat, Castaing & Chillà (2001) and by Hunt *et al.* (2003), but the form appropriate to the present considerations was determined by Verzicco (2004). Specifically, he wrote the Nusselt number for the infinitely conducting plates, Nu_{inf}, as

$$Nu_{inf} = Nu/F(X), \tag{3.1}$$

where X is the ratio of the effective thermal resistance of the fluid to that of the plate, given by

$$X = Nu^{-1}(k_p H)/(k_f e), \tag{3.2}$$

e being the plate thickness; k_p and k_f are the thermal conductivities of the plate and the fluid, respectively. The function $F(X)$ is fitted by

$$F(X) = 1 - \exp\left[-(X/4)^{1/3}\right] X/(X-2). \tag{3.3}$$

Recently, Brown *et al.* (2005) have examined the problem experimentally using a cylindrical cell with both copper and aluminium bounding plates. These authors, however, could not obtain a sufficient collapse of their data using $F(X)$ in the form (3.3), and so suggested a slightly modified functional form

$$F(X) = 1 - \exp[-(\alpha X)^{\beta}], \tag{3.4}$$

with $\alpha = 0.275$ and $\beta = 0.39$. Considering that this empirical relation was obtained for the same geometry as in our experiments, and also for aspect ratios larger than $1/2$, we adopt it here as the best available estimate for these plate effects. The maximum deviation in the correction factor using the two forms of $F(X)$ is 0.9 %, which could therefore be considered a measure of the uncertainty introduced by this procedure.

The effects of these corrections are shown in figure 1 for aspect ratios $1/2$, 1 and 4. The plates were identical for all cases and only the distance H between the plates changed. Other factors being equal, smaller H results in smaller thermal resistance of the fluid layer and hence in a smaller X for a given Ra. Numerical values of X are shown in the inset. The corrections in all cases are negligible over most of the range of Ra, the effect being measurable only over the last half a decade or so. Since the conditions are also non-Boussinesq in this range (see below), we have tended to rely less on those data, now as in the past.

3.2.2. *Sidewall conduction*

In conventional practice, the measured Nu is computed by subtracting from the total vertical heat flux a contribution due to parallel conduction up the sidewall, assuming the linear temperature gradient along its height to be $\Delta T/H$. The gradient is more complex in turbulent convection, and depends on the junction of the sidewalls and the horizontal plates. This effect has been modelled by Roche (2001), Ahlers (2001),

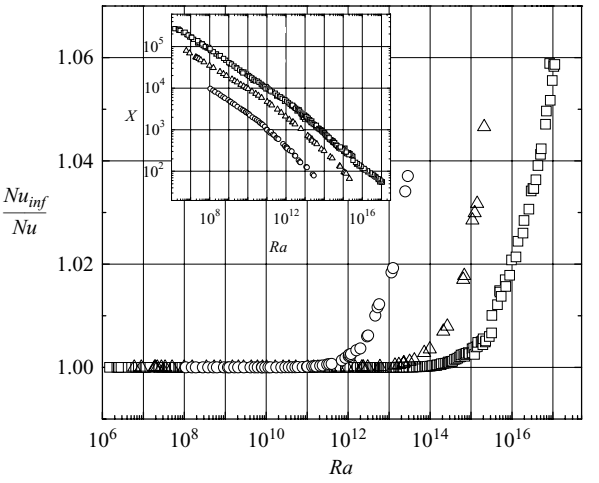

FIGURE 1. Ratio of Nu_{inf} to the measured Nu for convection cells of three different aspect ratios. Open squares, $\Gamma = 1/2$ (Niemela *et al.* 2000); open triangles, $\Gamma = 1$ (Niemela & Sreenivasan 2003*a*); open circles, $\Gamma = 4$ (present). The inset shows the ratio of total thermal resistance of the fluid layer to that of the plates.

Verzicco (2002) and Niemela & Sreenivasan (2003*a*). The numerical simulations of Verzicco, for $\Gamma = 1/2$, comparing simulations with perfectly insulating walls to those having walls of finite conductivity, indicate that, in the latter case, the forcing of the large-scale eddies is a predominant feature of the flow at low and moderate Ra, and leads to a larger overall heat transfer than for perfectly insulated walls. Given the complexity of the problem, it is not straightforward to extract the correction for an aspect ratio different from the one for which studies have specifically been made before. We use here a parameterization for extrapolating Nu to the limit of perfectly insulating walls put forward by Roche (2001) (see, also, Roche *et al.* 2001), because it has an explicit aspect ratio dependence, although it too is an approximate parameterization.

3.3. *The 'corrected' data*

The corrections just described are at best plausible and must be taken with some reserve. Fortunately, they are small for our data, which can be seen from table 1 by comparing the corrected Nusselt numbers, Nu_{corr}, obtained by multiplying the measured data by the two correction factors, one for each effect just described, with the directly measured data.

The sidewall corrections are present only for relatively low Ra and their effect is to lower the Nusselt numbers; those for finite conductivity of horizontal walls are prevalent only for high Ra and their effect is to enhance the Nusselt numbers. The cumulative effect is to increase the Nu–Ra slope compared to that for the uncorrected data. To illustrate this effect, we note that without corrections, a simple least-squares fit over the entire range of Ra for aspect ratio 1/2 (Niemela *et al.* 2000) gives a slope of 0.31, while the corrected data possess an average slope of 0.32 over the same range of Ra. These latter data are shown in figure 2 together with the fit. A similar plot for aspect ratio 4 is shown as figure 3. Again, the effect of corrections is small. The inset to figure 3 plots Nu_{corr} normalized by the one-third power of Ra. Clearly, there is a region of about 2 decades of Ra where Nu_{corr} is proportional roughly to $Ra^{1/3}$. The exponent can be inferred to be just barely higher than 1/3, being 0.34 over the range

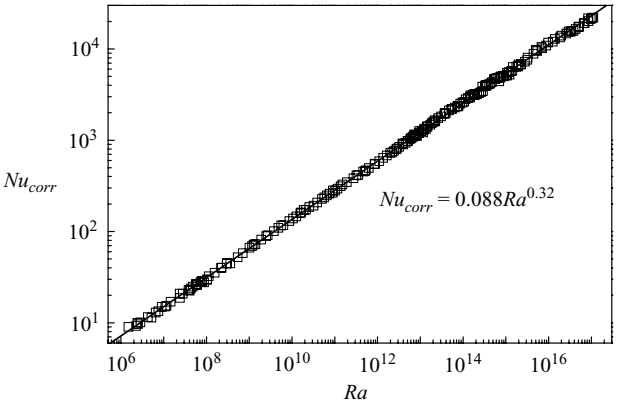

FIGURE 2. The heat transfer results for $\Gamma = 1/2$ 'corrected' here for sidewall leak and finite conductivity of horizontal plates. A linear least-square fit through the corrected data gives $Nu = 0.088Ra^{0.32}$, compared with $Nu = 0.124Ra^{0.31}$ for the directly measured Nu (Niemela *et al.* 2000).

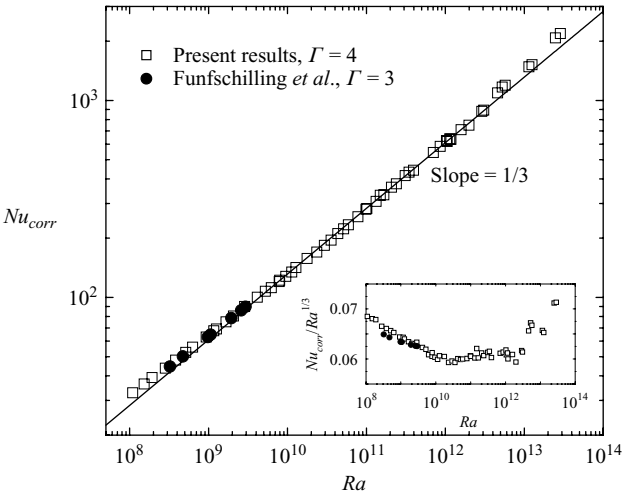

FIGURE 3. Nu_{corr} versus Ra for the present data ($\Gamma = 4$), adjusted for the effects of sidewall and horizontal plates. Also shown are recent results of Funfschilling *et al.* (2005) for aspect ratio 3, similarly corrected. The inset shows the same Nu_{corr} data normalized by $Ra^{1/3}$.

of $10^{10} < Ra < 10^{12}$, with the corrections described above raising the slope over the uncorrected data, which have a slope of more precisely $1/3$. For the data falling in the range $10^8 < Ra < 10^{10}$ the local log–log slope is nearly constant giving an exponent of 0.31. Both the constancy of the log–log slope with increasing Ra and its numerical value are in good agreement with predictions of Grossmann & Lohse (2002) in this range of Ra and for unity Pr (see their figure 4*b*). While the theory also predicts a saturation of the local exponent to $1/3$ at higher Ra, it occurs more slowly than is observed here. For comparison, we also show recent results of Funfschilling *et al.* (2005) also corrected for sidewall and end-plate effects. These data were obtained for $\Gamma = 3$ and $Pr = 4.38$, and accessed a limited range of Ra.

For $Ra > 3 \times 10^{12}$ the slope of the Nu–Ra curve increases significantly, as can be seen better in the inset to figure 3. However, it is precisely in this region of Ra

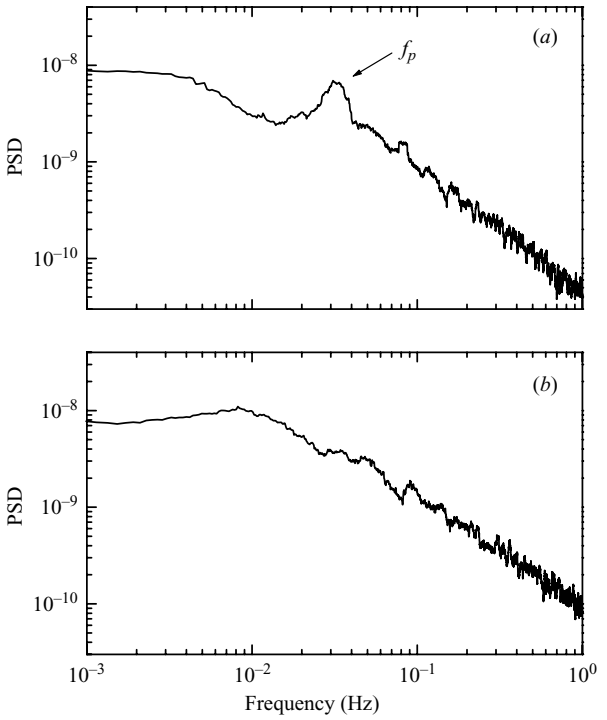

FIGURE 4. The power spectral density (PSD), for $Ra = 1.9 \times 10^9$, for temperature fluctuations measured (a) at the horizontal midplane of the apparatus along the sidewall and (b) in the centre. The peak in the sidewall data, labelled f_p, indicates the advection of plumes by a large-scale coherent wind. The broad and weak peak in (b) is roughly centred at $f_p/4$.

that conditions are not strictly Boussinesq,† as discussed in Niemela & Sreenivasan (2003*a*). We note that nearness to the critical state, which occurs at the highest *Ra*, indirectly may have important consequences for the heat transfer, as discussed in Niemela & Sreenivasan (2006). The near-critical state is also accompanied by a significant increase in *Pr*. Given our incomplete understanding of these effects, any definitive statement about the asymptotic power law, especially that approaching the value predicted by Kraichnan (1962), seems unjustified. As in Niemela & Sreenivasan (2003*a*), we err on the side of caution and do not draw major conclusions on that particular aspect. It is indeed possible that this increase in slope is genuine, but we do not know enough at present to be certain. A more detailed treatment of this feature of turbulent convection can be found in Niemela & Sreenivasan (2005).

3.4. *Temperature fluctuations and scaling*

We now turn to temperature fluctuations within the convection cell. Figure 4(*a*) shows the power spectral density (PSD) for $Ra = 1.9 \times 10^9$ at a point 4 cm inboard of the sidewall in the central horizontal plane; figure 4(*b*) is for the cell centre. Near the sidewall the plumes are advected by the mean wind (see e.g. Wu 1991; Cioni,

† The usual parameters characterizing non-Boussinesq effects became significant only for $Ra > 10^{15}$ for the $\Gamma = 1/2$ data of Niemela *et al.* (2000) and for $Ra > 10^{14}$ for the $\Gamma = 1$ data of Niemela & Sreenivasan (2003*a*), where these details are discussed fully. For the helium data of Chavanne *et al.* (2001) and Roche (2001), these effects occurred at much lower *Ra*.

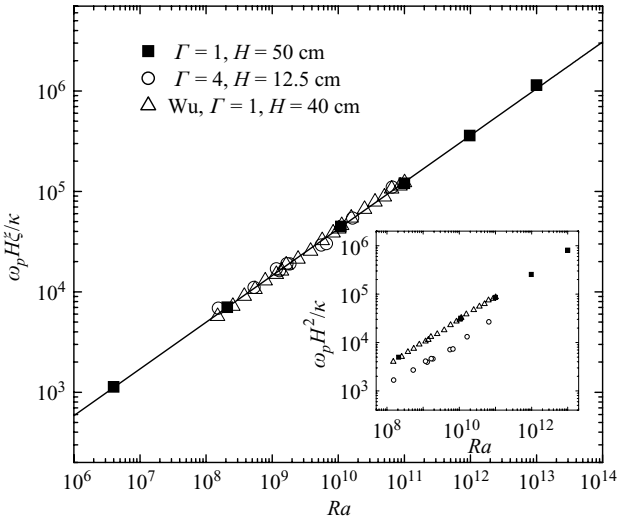

FIGURE 5. $\tilde{\omega}^*$ vs. Ra for various experiments $\Gamma \geqslant 1$ and Prandtl number $\simeq 0.7$. Open circles, present data, $\Gamma = 4$; solid squares, Niemela *et al.* (2001), $\Gamma = 1$; open triangles, Wu (1991), $\Gamma = 1$. Inset: Conventionally defined $\tilde{\omega}$ versus Ra for the same data sets, showing collapse only for the same aspect ratio. The line with slope 0.465 is the least-squares fit to the present data for $\Gamma = 1, 4$. After converting the dimensionless frequencies to a Reynolds number Re_f (see text) we obtain $Re_f Pr^{2/3} = 0.44 Ra^{0.45}$ (see (3.7)), whereas the scaling of the dimensionless frequency $\tilde{\omega}^*$ gives $\tilde{\omega}^* = 0.95 Ra^{0.465}$.

Ciliberto & Sommeria 1997; Niemela *et al.* 2001; Qui & Tong 2001; Sreenivasan, Bershadskii & Niemela 2002), which results in a prominent peak in the PSD, here at about $f_p = 0.033$ Hz. No such periodic feature exists for the other spectrum, corresponding to measurements at the centre, indicating the absence of plume advection by the coherent mean wind. These results are consistent with the early work of Krishnamurti & Howard (1981) for large aspect ratio and for considerably smaller Ra. We note, however, that there appears to be a broadened peak for the centre PSD at the frequency $f_p/4$. This could be due to a sloshing mode similar to that discussed by Sun, Xia & Tong (2005).

To make comparisons with data from other sources, it is customary to consider the dimensionless circular frequency $\tilde{\omega} = \omega_p H^2/\kappa \equiv 2\pi f_p H^2/\kappa$, using the vertical diffusion time as the scaling variable. The quantity $\tilde{\omega}$ is related to the advection rate for plumes – and hence can be related to the Reynolds number of the wind, which in turn is known to have a significant Prandtl number dependence (see figure 17 in Niemela & Sreenivasan 2003*a*). For constant Pr, we might expect to see a collapse of the data for various experiments. This does not happen, however, as shown in the inset to figure 5: while the data of Wu (1991) and Niemela *et al.* (2001) for $\Gamma = 1$ collapse well using this standard normalization, the present results for $\Gamma = 4$ fall considerably below. We surmize that a length scale different from the vertical height is appropriate for scaling $\tilde{\omega}$. If a single coherent mean wind encompasses the entire container† we may expect that the horizontal dimension might also be important for scaling. From what we know of the wind we can choose (half) the perimeter of the

† This is in contrast to the situation at the onset of convection, where the individual rolls are roughly square in cross-section and scale with the vertical distance between the horizontal plates.

apparatus in section, namely $H + D$, or alternatively, considering the tilted nature of the wind (Qui & Tong 2001; Niemela & Sreenivasan 2003*b*; Xia, Sun & Zhou 2003), choose the 'diagonal' measure of the container defined as

$$\xi = (H^2 + D^2)^{1/2}. \tag{3.5}$$

Using the latter we write a new dimensionless representation $\tilde{\omega}^*$ of the plume advection frequency, for fixed Pr, as

$$\tilde{\omega}^* = \omega_p \, \xi H/\kappa = \tilde{\omega} \, [1 + \Gamma^2]^{1/2}. \tag{3.6}$$

We show in figure 5 the collapse of the data using this scaling. The perimeter works almost as well as the diagonal. If the wind followed the walls closely, the perimeter would seem to be relevant scale, while if it were tilted along the diagonal, the relevant scale would be ξ. The evolution of the wind from one shape to the other has been discussed in Niemela & Sreenivasan (2003*b*) and Xia *et al.* (2003). Unfortunately, the range of Ra used in figure 5 is unable to establish the superiority of one scale over the other. This suggests that, on the average, the wind probably possesses an in-between orientation and evolves rather slowly for the range of Ra covered here.

In general, neither normalization can be expected to work for aspect ratios far below unity because the flow may then admit stacked cells which alters the scaling.

We can also define a quantity that is related to a Reynolds number (see e.g. Niemela *et al.* 2001; Qui & Tong 2001; Lam *et al.* 2002), namely $Re_f^* = (1/\pi)\tilde{\omega}^* Pr^{-1}$. A least-squares fit to the data gives

$$Re_f^* Pr^{2/3} = 0.44 Ra^{0.453}. \tag{3.7}$$

This scaling of the Γ-independent Re_f^* is in excellent agreement with the predicted scaling of the Reynolds number $Re \sim Ra^{4/9} Pr^{-2/3}$ in the Pr–Ra phase space region IV_u of Grossmann & Lohse (2001) and with similar experimental results of Qui & Tong (2001) and those of Lam *et al.* (2002). We note that choosing the empirical $Pr^{-0.76}$ dependence of the latter authors does not change the result significantly, giving $Re_f^* = 0.39 Ra^{0.456} Pr^{-0.76}$. We cannot resolve any Ra-dependence of the Pr-exponent but note that this dependence is negligible in the theoretical results for Pr of order unity (see figure 4*a* of Grossmann & Lohse 2002), as in the experiments. The least-squares fit to the $\tilde{\omega}^*$ data gives $\tilde{\omega}^* = 0.95 Ra^{0.465}$.

Finally, we illustrate in figure 6 the nature of correlations between sensor pairs for temperature sensors placed the same distance from the sidewall on opposite ends of a diameter (i.e. separated azimuthally by π radians) and that between a sidewall sensor and one centred at the midpoint of the cell. In figure 6(*a*), both such correlations are shown for $Ra = 3.1 \times 10^9$, i.e. in the region of logNu–logRa slope 0.31. It is clear that there is a strong long-time correlation between opposite sidewall sensors, indicative of a well ordered and robust mean wind, while no clear correlation exists between the sidewall fluctuations and those of the centre. This corroborates the lack of any strong mean wind in the centre. Figure 6(*b*) shows the same correlations for a higher $Ra = 6.5 \times 10^{11}$, well into the region of approximate logNu–logRa slope 1/3. Here, it can be appreciated that there is no correlation between any set of temperature signals, indicating that the mean wind is no longer coherent over the entire container. We point out here that this latter observation is consistent with the assumption of uncoupled boundary layers from which a 1/3 power-law exponent naturally derives (see e.g. Howard 1966).

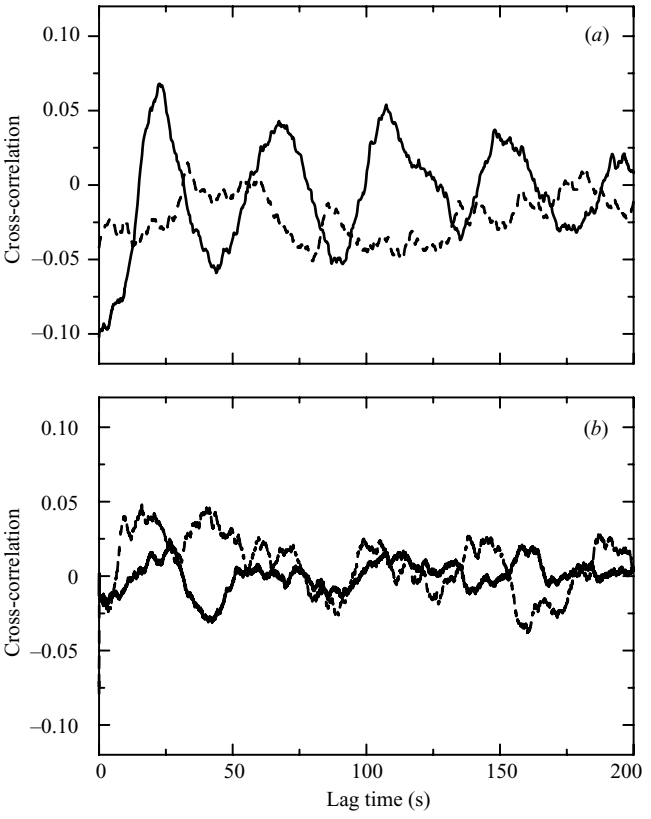

FIGURE 6. (*a*) Cross-correlation of temperatures for $Ra = 3.1 \times 10^9$. Solid line, correlation between sidewall temperatures at the midplane but at opposite ends of a cell diameter; dashed line, correlation between a sidewall temperature and that at the centre of the cell. (*b*) Similar cross-correlation of temperatures for $Ra = 6.5 \times 10^{11}$.

4. Concluding remarks

We have reported heat transfer and temperature fluctuation data for aspect ratio 4 with Ra up to 2×10^{13}. For $10^8 < Ra < 10^{10}$, the logNu–logRa slope is nearly constant and of magnitude 0.31. For higher Ra it saturates at around $1/3$ in the range of Ra for which the Boussinesq limit is valid strictly, as in Niemela & Sreenivasan (2003*a*), and in recent experiments by Nikolaenko *et al.* (2005). The corrected data suggest a marginally higher slope than $1/3$, namely 0.34, but these corrections are at best approximate – and fortunately relatively small – so we do not give special significance to this slight difference. The increase in slope for higher Ra is less subtle, but the possible non-Boussinesq effects and the Pr variations in that range of Ra prevent us from drawing serious conclusions. In fact, we prefer to remain on the side of caution, and do not wish to comment on the claims of Chavanne *et al.* (2001), who used data in the region of strong non-Boussinesq effects and Pr-variations to infer an approach to the $1/2$ power.

Finally, the peak in the temperature fluctuation spectrum measured near the sidewall, corresponding to plume advection by the coherent mean wind, scales well in experiments with different aspect ratios if a diagonal measure of the cell is considered as the characteristic length scale. Using the perimeter as the scale also works nearly as well. This ambiguity is consistent with our understanding of the wind as generally

tilted but slowly evolving to a squarish shape at higher *Ra* (Niemela & Sreenivasan 2003*b*; Xia *et al.* 2003). Either scaling reinforces the notion of a single, coherent mean wind that, on the average, encompasses the entire container. At very high *Ra*, however, the mean wind can no longer be considered coherent over the container as indicated by a lack of long-time correlation between opposite sidewall sensors. This is the *Ra*-range where the power law is closely 1/3. Finally, a Γ-independent Reynolds number based on the frequency peak in the power spectral density of the mean wind is in excellent agreement with the theoretical predictions of Grossmann & Lohse (2001, 2002).

We thank the Elettra Synchrotron Light Laboratory, Trieste, for providing laboratory space, and the National Science Foundation grant DMR 0202554 for support in the construction of the apparatus.

REFERENCES

Ahlers, G. 2001 Effect of sidewall conductance on heat-transport measurements for turbulent Rayleigh-Benard convection. *Phys. Rev.* E **63**, 015303.

Amati, G., Koal, K., Massaioli, F., Sreenivasan, K. R. & Verzicco, R. 2005 Turbulent thermal convection at high Rayleigh numbers for a Boussinesq fluid of constant Prandtl number. *Phys. Fluids* **17**, 121701.

Brown, E., Nikolaenko, A., Funfschilling, D. & Ahlers, G. 2005 Heat transprt in turbulent Rayleigh-Benard convection: Effect of finite top- and bottom-plate conductivity. *Phys. Fluids* **17**, 075108.

Chaumat, S., Castaing, B. & Chillà, F. 2002 Rayleigh-Bénard cells: influence of the plates properties. In *Advances in Turbulence IX, Proc. Ninth European Turbulence Conference* (ed. I. P. Castro & P. E. Hancock). CIMNE, Barcelona.

Chavanne, X., Chilla, F., Chabaud, B., Castaing, B. & Hebral, B. 2001 Turbulent Rayleigh-Bénard convection in gaseous and liquid He. *Phys. Fluids* **13**, 1300–1320.

Chilla, F., Rastello, M., Chaumat, S. & Castaing, B. 2004 Long relaxation times and tilt sensitivity in Rayleigh Bénard turbulence. *Eur. Phys. J.* B **40**, 223–227.

Cioni, S., Ciliberto, S. & Sommeria, J. 1997 Strongly turbulent Rayleigh-Bénard convection in mercury: comparison with results at moderate Prandtl number. *J. Fluid Mech.* **335**, 111–140.

Funfschilling, D., Brown, E., Nikolaenko, A. & Ahlers, G. 2005 Heat transport by turbulent Rayleigh-Benard convection in cylindrical samples with aspect ratio one and larger. *J. Fluid Mech.* **536**, 145–154.

Goldstein, R. J. & Tokuda, S. 1979 Heat transfer by thermal convection at high Rayleigh numbers. *Intl J. Heat Mass Transfer* **23**, 738–740.

Grossmann, S. & Lohse, D. 2001 Thermal convection fo large Prandtl numbers. *Phys. Rev. Lett.* **86**, 3316–3319.

Grossmann, S. & Lohse, D. 2002 Prandtl and Rayleigh number dependence of the Reynolds number in turbulent thermal convection. *Phys. Rev.* E. **66**, 016305.

Howard, L. N. 1966 Convection at high Rayleigh number. *Proc. Eleventh Intl Congress on Applied Mechanics* (ed. H. Görtler), pp. 1109–1115. Springer.

Hunt, J. C. R., Vrieling, A. J., Nieuwstadt, F. T. M. & Fernando, H. J. S. 2003 The influence of the thermal diffusivity of the lower boundary on eddy motion in convection. *J. Fluid Mech.* **491**, 183–205.

Krishnamurti, R. & Howard, L. N. 1981 Large-scale flow generation in turbulent convection. *Proc. Natl Acad. Sci.* **78**, 1981–1985.

Lam, S., Shang, X.-D., Zhou, S.-Q. & Xia, K.-Q. 2002 Prandlt number dependence of the viscous boundary layer and the Reynolds numbers in Rayleigh-Bénard convection *Phys. Rev. Lett.* **65**, 066306.

Niemela, J. J., Skrbek, L., Sreenivasan, K. R. & Donnelly, R. J. 2000 Turbulent convection at very high Rayleigh numbers. *Nature* **404**, 837–840.

Niemela, J. J., Skrbek, L., Sreenivasan, K. R. & Donnelly, R. J. 2001 The wind in confined thermal convection. *J. Fluid Mech.* **449**, 169–178.

Niemela, J. J. & Sreenivasan, K. R. 2003*a* Confined turbulent convection *J. Fluid Mech.* **481**, 355–384.

Niemela, J. J. & Sreenivasan, K. R. 2003*b* Rayleigh number evolution of large scale coherent motion in turbulent convection. *Europhys. Lett.* **62**, 829–833.

Niemela, J. J. & Sreenivasan, K. R. 2006 Heat transport in near-critical helium. In preparation.

Nikolaenko, A., Brown, E., Funfschilling, D. & Ahlers, G. 2005 Heat transport by turbulent Rayleigh-Benard convection in cylindrical cells with aspect ratio one and less. *J. Fluid Mech.* **523**, 251–260.

Qiu, X.-L. & Tong, P. 2001 Large-scale structures in turbulent thermal convection. *Phys. Rev.* E **64**, 036304.

Roche, P. E. 2001 Convection thermique turbulente en cellule de Rayleigh-Bènard cryogénique. PhD thesis, Centre de Recherche sur les Trés Basses Températures Laboratoire CNRS associé á l'Université Joseph Fourier.

Roche, P., Castaing, B., Chabaud, B., Hebral, B. & Sommeria, J. 2001 Sidewall effects in Rayleigh-Bénard convection. *Eur. Phys. J.* **24**, 405–408.

Sreenivasan, K. R. & Donnelly, R. J. 2000 Role of cryogenic helium in classical fluid dynamics: basic research and model testing. *Adv. Appl. Mech.* **37**, 239–275.

Sreenivasan, K. R., Bershadskii, A. & Niemela, J. J. 2002 Mean wind and its reversal in thermal convection. *Phys. Rev.* E **65**, 056306.

Sun, C., Xia, K.-Q. & Tong, P. 2005 Three-dimensional flow structures and dynamics of turbulent thermal convection in a cylindrical cell. *Phys. Rev.* E **72**, 026302.

Tritton, D. J. 1988 *Physical Fluid Dynamics.* Clarendon.

Verzicco, R. 2002 Side wall finite conductivity effects in confined turbulent thermal convection. *J. Fluid Mech.* **473**, 201–210.

Verzicco, R. & Camussi, R. 2003 Numerical experiments on strongly turbulent thermal convection in a slender cylindrical cell. *J. Fluid Mech.* **477**, 19–49.

Verzicco, R. 2004 Effects of nonperfect thermal sources in turbulent thermal convection *Phys. Fluids* **16**, 1965.

Wu, X.-Z. & Libchaber, A. 1992 Scaling relations in thermal turbulence: The aspect-ratio dependence. *Phys. Rev.* A **45**, 842–845.

Wu, X.-Z. 1991 Along the road to developed turbulence: free thermal convection in low temperature helium. PhD thesis, University of Chicago.

Xia, K.-Q., Sun, C. & Zhou, S.-Q. 2003 Particle image velocity measurement of the velocity field in turbulent thermal convection. *Phys. Rev.* E **68**, 066303.

Zhou, S. Q. & Xia, K.-Q. 2002 Plume statistics in thermal turbulence: Mixing of an active scalar. *Phys. Rev. Lett.* **89**, 184502.